The Updated Registry of Fast Myocardial Perfusion Imaging with Next-Generation SPECT (REFINE SPECT 2.0)

Robert J.H. Miller[1,2], Mark Lemley[1], Aakash Shanbhag[1], Giselle Ramirez[1], Joanna X. Liang[1], Valerie Builoff[1], Paul Kavanagh[1], Tali Sharir[3], M. Timothy Hauser[4], Terrence D. Ruddy[5], Mathews B. Fish[6], Timothy M. Bateman[7], Wanda Acampa[8], Andrew J. Einstein[9], Sharmila Dorbala[10], Marcelo F. Di Carli[10], Attila Feher[11], Edward J. Miller[11], Albert J. Sinusas[11], Julian Halcox[12], Monica Martins[12], Philipp A. Kaufmann[13], Damini Dey[1], Daniel S. Berman[1], and Piotr J. Slomka[1]

[1]Division of Artificial Intelligence in Medicine, Departments of Medicine, Biomedical Sciences, and Imaging, Cedars–Sinai Medical Center, Los Angeles, California; [2]Department of Cardiac Sciences, University of Calgary and Libin Cardiovascular Institute, Calgary, Alberta, Canada; [3]Department of Nuclear Cardiology, Assuta Medical Centers, Tel Aviv, Israel, and Ben Gurion University of the Negev, Beer Sheba, Israel; [4]Department of Nuclear Cardiology, Oklahoma Heart Hospital, Oklahoma City, Oklahoma; [5]Division of Cardiology, University of Ottawa Heart Institute, Ottawa, Ontario, Canada; [6]Oregon Heart and Vascular Institute, Sacred Heart Medical Center, Springfield, Oregon; [7]Cardiovascular Imaging Technologies LLC, Kansas City, Missouri; [8]Department of Advanced Biomedical Sciences, University of Naples, Naples, Italy; [9]Division of Cardiology, Department of Medicine, and Department of Radiology, Columbia University Irving Medical Center and New York–Presbyterian Hospital, New York, New York; [10]Division of Nuclear Medicine and Molecular Imaging, Department of Radiology, Brigham and Women's Hospital, Boston, Massachusetts; [11]Section of Cardiovascular Medicine, Department of Internal Medicine, Yale University School of Medicine, New Haven, Connecticut; [12]Swansea University Medical School, Swansea University, Swansea, United Kingdom; and [13]Cardiac Imaging, Department of Nuclear Medicine, University Hospital Zurich, Zurich, Switzerland

The Registry of Fast Myocardial Perfusion Imaging with Next-Generation SPECT (REFINE SPECT) has been expanded to include more patients and CT attenuation correction imaging. We present the design and initial results from the updated registry. **Methods:** The updated REFINE SPECT is a multicenter, international registry with clinical data and image files. SPECT images were processed by quantitative software and CT images by deep learning software detecting coronary artery calcium (CAC). Patients were followed for major adverse cardiovascular events (MACEs) (death, myocardial infarction, unstable angina, late revascularization). **Results:** The registry included scans from 45,252 patients from 13 centers (55.9% male, 64.7 ± 11.8 y). Correlating invasive coronary angiography was available for 3,786 (8.4%) patients. CT attenuation correction imaging was available for 13,405 patients. MACEs occurred in 6,514 (14.4%) patients during a median follow-up of 3.6 y (interquartile range, 2.5–4.8 y). Patients with a stress total perfusion deficit of 5% to less than 10% (unadjusted hazard ratio [HR], 2.42; 95% CI, 2.23–2.62) and a stress total perfusion deficit of at least 10% (unadjusted HR, 3.85; 95% CI, 3.56–4.16) were more likely to experience MACEs. Patients with a deep learning CAC score of 101–400 (unadjusted HR, 3.09; 95% CI, 2.57–3.72) and a CAC of more than 400 (unadjusted HR, 5.17; 95% CI, 4.41–6.05) were at increased risk of MACEs. **Conclusion:** The REFINE SPECT registry contains a comprehensive set of imaging and clinical variables. It will aid in understanding the value of SPECT myocardial perfusion imaging, leverage hybrid imaging, and facilitate validation of new artificial intelligence tools for improving prediction of adverse outcomes incorporating multimodality imaging.

Key Words: SPECT; solid-state detector; myocardial perfusion imaging; coronary artery disease; artificial intelligence; quantitative analysis

J Nucl Med 2024; 65:1795–1801
DOI: 10.2967/jnumed.124.268292

Coronary artery disease (CAD) is the leading cause of death in the United States in both men and women and remains a significant public health problem worldwide (*1*). SPECT myocardial perfusion imaging (MPI) is established as a valuable diagnostic tool to evaluate patients with diagnosed or suspected CAD (*2*). Over 15 million MPI studies are performed annually worldwide (*3*).

We previously developed a registry for next-generation SPECT scanners, the Registry of Fast Myocardial Perfusion Imaging with Next-Generation SPECT (REFINE SPECT) (*4*). This registry has a novel collaborative design with the contribution of clinical data and image datasets from centers worldwide combined into a comprehensive database established at the central core laboratory. The REFINE SPECT registry has demonstrated the value of automated assessments of perfusion (*5*), functional parameters (*6,7*), and phase analysis (*8*) while also providing insights into specific comorbidities (*9,10*). Additionally, the registry has been used to outline the potential benefits of applying artificial intelligence to integrate all this information (*11,12*). Over 35 publications have been aided by the REFINE SPECT registry to date.

However, since REFINE SPECT was developed, the importance of adjunctive CT imaging (acquired for attenuation correction [AC] or separate dedicated [CTAC] scans) has been recognized (*13*), performed often with conventional-geometry scanners. This information can improve SPECT MPI's diagnostic and prognostic accuracy. CTAC imaging also provides valuable opportunities to assess coronary artery calcification (*14–17*) or identify other intrathoracic pathology (*18*). Additionally, the original registry was too small to assess some subgroups (such as patients with peripheral artery

Received Jun. 25, 2024; revision accepted Sep. 9, 2024.
For correspondence or reprints, contact Piotr Slomka (piotr.slomka@cshs.org).
Published online Oct. 3, 2024.

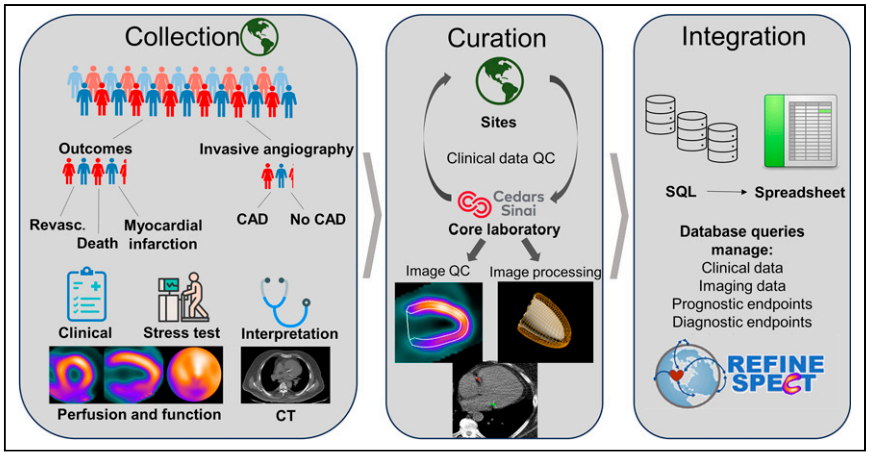

FIGURE 1. Overview of data acquisition and processing scheme for REFINE SPECT registry. Activities include clinical data and image collection, deidentification at participating sites, data transfer to core laboratory for further data-processing quality control in communication with sites, batch mode image quantification, and combined database integration. SQL = structured query language; QC = automatic quality control.

disease) and did not include contemporary patient populations. As a result, it is critical to update REFINE SPECT to ensure its wide applicability and validity for contemporary SPECT MPI. This report describes the rationale, design, and initial data characteristics of the updated REFINE SPECT registry.

MATERIALS AND METHODS

Overall Study Design

The study objective was to build an imaging registry of patient-level new-generation SPECT MPI data—the REFINE SPECT registry—which includes rich clinical data, stress testing, imaging datasets, and correlating follow-up information (*4*). The registry reflects the clinical routine of the investigative centers and uses a collaborative design with the contribution of both clinical data and image datasets to the registry (Fig. 1). Additional details are available in the supplemental materials (supplemental materials are available at http://jnm.snmjournals.org).

The investigators asked the institutional ethics committee at each center to evaluate and approve the study protocol before data collection and transfer. In addition, the investigational review board at Cedars–Sinai Medical Center approved the overall data collection for the registry. The study complied with the Declaration of Helsinki, and sites either obtained written informed consent or a waiver of consent for the use of the deidentified data.

Patient Population

The cohort included consecutive patients at each center referred for SPECT imaging, with scans performed between 2009 and 2021. The collected clinical variables are shown in Supplemental Table 1. Investigative centers performed Health Insurance Portability and Accountability Act–complaint deidentification of the data; the central core laboratory did not receive any information that would directly or indirectly identify the study patients.

Diagnostic Outcomes

The diagnostic population from the registry included patients who had known CAD who underwent invasive angiography within 6 mo of the MPI. Invasive coronary angiography results and revascularization details were collected from medical records using site-specific methods. Stenosis severity was recorded separately for each available coronary segment and in most cases was based on visual stenosis estimation from the interpreting cardiologist at the time of invasive angiography. A stenosis severity of at least 70% in the left anterior descending artery, left circumflex artery, or right coronary artery, or of at least 50% in the left main coronary artery, was considered significant.

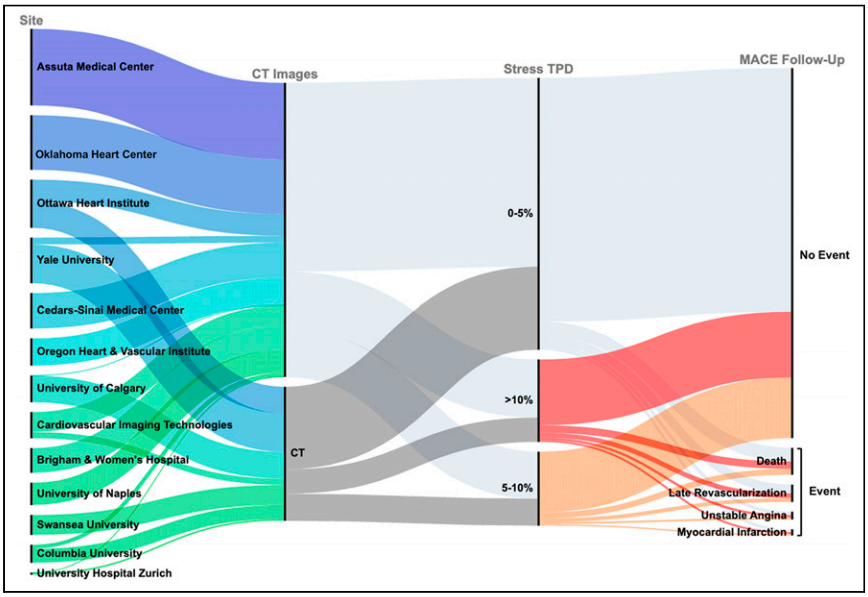

FIGURE 2. Sankey diagram outlining distribution of patients. Line width is proportional to number of patients. MACEs included death, revascularization (with early revascularization defined as ≤90 d from scan), myocardial infarction, or admission for unstable angina.

Prognostic Outcomes

The primary clinical outcome for the registry was major adverse cardiovascular events (MACEs), which comprised all-cause mortality, nonfatal myocardial infarction, unstable angina, or late coronary revascularization. Early revascularization was defined as revascularization no more than 90 d after SPECT imaging, and late revascularization was defined as any revascularization occurring more than 90 d after SPECT imaging (*19*). Unstable angina was defined on the basis of hospital admission for a recent onset or worsening of chest pain and diagnostics suggesting myocardial ischemia. Nonfatal myocardial infarction was defined as hospital admission for a recent onset or worsening of chest pain with elevated cardiac enzyme levels and ischemic electrocardiography changes (*20*). Details of follow-up ascertainment by site are available in the supplemental materials.

SPECT Imaging Acquisition and Reconstruction

Studies were typically acquired using 2 imaging positions (supine/prone or upright/supine) or

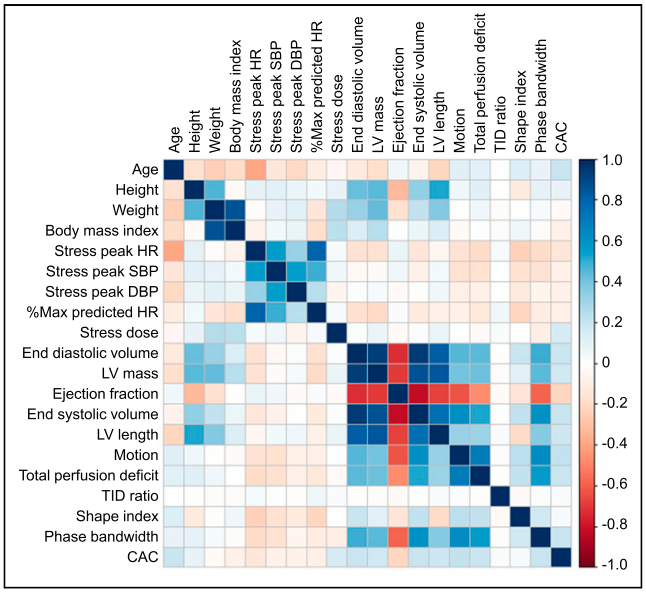

FIGURE 3. Correlation between clinical, stress, and stress imaging variables. Darker blue indicates higher positive correlation, and darker red indicates higher negative correlation. DBP = diastolic blood pressure; HR = heart rate; LV = left ventricle; SBP = systolic blood pressure; TID = transient ischemic dilation.

1 position with and without attenuation correction for the SPECT/CT systems, with both image sets sent to the registry when available. Reconstructed images were derived by vendor-recommended iterative reconstruction optimized for each scanner at each participating site. If CTAC scans were obtained, these images were also collected and transferred to the registry for core laboratory analysis.

CT Imaging Acquisition and Reconstruction

CT images were acquired with the site-specific imaging protocols in Supplemental Table 2.

Clinical MPI Reporting

Expert visual interpretation was performed during clinical reporting as outlined in the supplemental materials.

Image Database

Image datasets were reconstructed and deidentified on-site as outlined in the supplemental materials.

Core Laboratory Processes

Quality Control. The deidentified image files were quality control–checked by experienced core laboratory technologists without knowledge of the clinical data; further details are in the supplemental materials.

SPECT Quantification. After quality control, images were quantified in quantitative perfusion SPECT or quantitative gated SPECT using a consistent batch-processing mode. The software outputs a single row of the image variables (including perfusion, functional, and morphologic measures) quantified per image dataset. In patients with available CT, this quantification was performed with and without attenuation correction. If applicable, combined perfusion parameters (computed from 2 positions) and ischemic perfusion deficit (difference between stress and rest) were also included (*21*).

CT Quantification. For CT attenuation scan acquisitions, regardless of the use of electrocardiogram gating, coronary artery calcium (CAC) was annotated by expert technicians including total score as well as individual scores for the left main, left anterior descending, left circumflex, and right coronary arteries. Deep learning was also applied (*15*) to automatically derive a total and heart-specific calcium score from the CT attenuation scans. Noncoronary calcification, including the ascending aorta, descending aorta, aortic valve, and mitral valve regions, was also annotated. There are 4 categories of CT variables, including a total of

TABLE 1
Characteristics of Diagnostic Cohort

Characteristic	No obstructive CAD (n = 1,568)	Obstructive CAD (n = 2,218)	*P*
Age (y)	64 (57–72)	67 (59–74)	<0.001
Male	888 (56.6)	1,635 (73.7)	<0.001
Body mass index (kg/m^2)	29.3 (25.5–33.5)	28.3 (25.2–32.1)	<0.001
Diabetes	434 (27.7)	794 (35.8)	<0.001
Hypertension	1,036 (66.1)	1,557 (70.2)	0.007
Dyslipidemia	766 (48.9)	1,213 (54.7)	<0.001
Current smoker	445 (28.4)	666 (30.0)	0.270
Family history of CAD	509 (32.5)	795 (35.8)	0.031
Peripheral artery disease	179 (11.4)	399 (18.0)	<0.001
Chest pain typicality			
Nonanginal	192 (12.2)	243 (11.0)	0.221
Atypical	514 (32.8)	720 (32.5)	0.837
Typical	149 (9.5)	380 (17.1)	<0.001
Exercise stress	694 (44.3)	1,160 (52.3)	<0.001
Stress TPD	4.1 (1.8–7.8)	10.4 (5.0–18.9)	<0.001

Obstructive CAD was defined as stenosis ≥ 50% in left main or ≥ 70% in any other coronary artery. Continuous variables are reported as median and interquartile range; categoric variables are reported as number and percentage.

16 variables overall. In this report, all CAC values are derived automatically using a deep learning model that was previously developed in a separate population (*22*). The deep learning model was developed in a subset of 500 patients from one site and integrates slice thickness into CAC calculation to allow for differences between studies. The deep learning CAC scores agreed well with expert CAC scores in the external populations (which had different acquisition parameters), with a Cohen κ of 0.80.

Imaging Variables. In total, 30 imaging variable categories including general imaging, perfusion, functional, and CT parameters were automatically quantified (Supplemental Table 3). These variable categories included separate values for stress/rest and static/gated scans, as well as values by regional and 17-segment models (over 290 variables if standard per-vessel regions were used and over 3,500 if 17-segment variables were considered). The processing time in batch mode was approximately 2.1 s for each complete patient case.

RESULTS

Patient Characteristics

To date, the REFINE SPECT registry includes 13 participating centers and 45,252 patients as shown in Supplemental Table 4. An overview of the data available for each site, as well as the distribution of early revascularization and MACE outcomes, is shown in Figure 2. The distribution of selected clinical and imaging parameters is shown in Supplemental Figure 1. Correlations between clinical, stress, and imaging variables are shown in Figure 3. The relationship between AC and non-AC stress total perfusion deficit (TPD) is shown in Supplemental Figure 2.

Diagnostic Outcomes

In total, 3,786 (8.4%) patients without known CAD underwent invasive angiography within 6 mo of MPI. Of those patients,

TABLE 2
Characteristics of Prognostic Cohort

Characteristic	MACEs (n = 6,514)	No MACEs (n = 38,738)	*P*
Age (y)	70 (61–77)	64 (56–72)	<0.001
Male	4,244 (65.2)	21,073 (54.4)	<0.001
Body mass index (kg/m^2)	27.8 (24.7–32.0)	28.4 (25.1–32.7)	<0.001
Race*			
American Indian or Native Alaskan	19 (0.8)	124 (0.8)	0.762
Asian	59 (2.4)	457 (2.8)	0.449
Black or African American	339 (13.6)	2,170 (13.3)	0.310
Native Hawaiian or Pacific Islander	5 (0.2)	36 (0.2)	0.958
White	1,875 (75.3)	12,019 (73.6)	0.745
Multiracial	46 (1.9)	376 (2.3)	0.410
Diabetes	2,359 (36.2)	9,918 (25.6)	<0.001
Hypertension	4,489 (69.7)	24,445 (63.2)	<0.001
Dyslipidemia	3,420 (53.3)	19,633 (50.9)	<0.001
Current smoker	1,694 (26.0)	9,147 (23.6)	<0.001
Peripheral artery disease	1,530 (23.5)	7,174 (18.5)	<0.001
Prior CAD	2,609 (40.0)	8,171 (21.1)	<0.001
Previous myocardial infarction	1,279 (19.6)	3,993 (10.3)	<0.001
Previous PCI or stent	1,667 (25.6)	5,459 (14.1)	<0.001
Previous CABG	884 (13.6)	2,300 (5.9)	<0.001
Chest pain typicality			
Nonanginal	881 (13.5)	7,559 (19.5)	<0.001
Atypical	1,481 (22.7)	10,850 (28.0)	<0.001
Typical	404 (6.2)	2,476 (6.4)	<0.001
Imaging acquisition			
Rest–stress on same day	3,264 (54.7)	20,883 (53.9)	0.497
Stress–rest on same day	1,605 (24.5)	8,346 (21.5)	<0.001
Stress and rest on separate days	689 (10.6)	1,485 (3.8)	<0.001
Stress only	956 (14.7)	8,024 (20.7)	<0.001
Exercise stress†	2,658 (40.8)	21,052 (54.3)	<0.001

*Race information was available in subset of 18,832 patients.
†Includes pharmacologic stress with low-level exercise.
PCI = percutaneous coronary intervention; CABG = coronary artery bypass grafting.
Continuous variables are reported as median and interquartile range; categoric variables are reported as number and percentage.

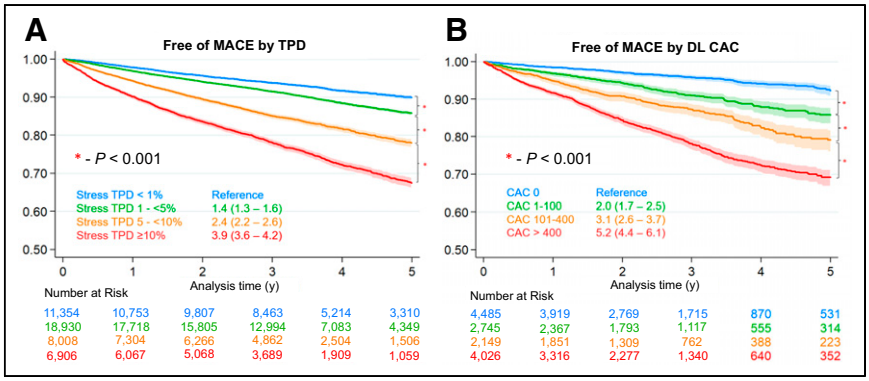

FIGURE 4. Survival free of MACEs. Curves are stratified by categories of stress TPD (A) and deep learning (DL) CAC (B). Shaded regions represent 95% CIs. MACEs included all-cause mortality, nonfatal myocardial infarction, admission for unstable angina, or revascularization.

obstructive CAD (defined as left main coronary artery ≥50% or ≥70% in other coronary arteries) was identified in 2,218 (58.6%). Patient characteristics stratified by the presence or absence of obstructive CAD are shown in Table 1. Predictive performance for obstructive CAD using TPD, CAC, or a model including both is shown in Supplemental Figure 3.

Prognostic Outcomes

MACEs occurred in 6,514 (14.4%) patients during a median follow-up of 3.6 y (interquartile range, 2.5–4.8 y). Patient characteristics stratified by the presence of MACEs are shown in Table 2. Survival free of MACEs, stratified by stress TPD, is shown in Figure 4A. Compared with patients with a stress TPD of less than 1%, patients with a stress TPD of 1% to less than 5% (unadjusted hazard ratio [HR], 1.44; 95% CI, 1.34–1.56), a stress TPD of 5% to less than 10% (unadjusted HR, 2.42; 95% CI, 2.24–2.62), and a stress TPD of 10% or higher (unadjusted HR, 3.85; 95% CI, 3.56–4.16) were more likely to experience MACEs.

Among the patients with available CT information (n = 13,405), MACEs occurred in 1,509 (11.3%) patients during a median follow-up of 2.4 y (interquartile range, 1.4–3.6 y). The characteristics for patients with available CT information are shown in Supplemental Table 5. An increasing deep learning CAC was associated with a higher risk of MACEs (Fig. 4B). Compared with patients with a deep learning CAC of 0, those with a CAC of 1–100 (unadjusted HR, 2.03; 95% CI, 1.68–2.46), a CAC of 101–400 (unadjusted HR, 3.09; 95% CI, 2.57–3.72), and a CAC of more than 400 (unadjusted HR, 5.17; 95% CI, 4.41–6.05) were at increased risk of MACEs. In patients with deep learning CAC and stress AC TPD images, patients with a stress AC TPD of 1% to less than 5% (unadjusted HR, 1.26; 95% CI, 1.06–1.49), a stress AC TPD of 5% to less than 10% (unadjusted HR, 1.53; 95% CI, 1.27–1.84), and a stress AC TPD of 10% or higher (unadjusted HR, 2.21; 95% CI, 1.85–2.64) were more likely to experience MACEs (Supplemental Fig. 4). Associations with the components of MACEs are shown in Supplemental Table 6.

DISCUSSION

We have established a large international imaging registry and derived a rich set of 28 clinical data variables, 19 stress test variables, and 30 imaging variable categories (comprising over 3,500 imaging variables when regional and segmental values are considered). However, since images are available for each study patient, there is no limit to the number of novel imaging variables that could be evaluated in the future. The registry is now enriched with multimodality imaging and a range of contemporary imaging protocols. Using automated image analysis, we demonstrated that even minimal perfusion deficits are associated with an increased risk of MACEs, with a greater risk of MACEs when there is a more extensive stress perfusion abnormality and a higher deep learning CAC. The REFINE SPECT registry will serve as an ideal source for evaluating novel imaging parameters and developing and validating clinically relevant artificial intelligence tools.

A variety of collaborative projects has resulted from the original REFINE SPECT registry. The large, diverse patient population is ideal for evaluating the diagnostic or prognostic utility of quantitative imaging parameters. For example, we have demonstrated that stress TPD provides incremental risk prediction over visual assessment of perfusion (*5*), and ischemic TPD can be used to identify patients who may derive MACE benefits from revascularization (*23*). In our preliminary data, there is clear stratification for the probability of obstructive CAD and the risk of MACEs with both increasing visual perfusion abnormality and increasing stress TPD. These data can also be used to show similar findings in important subgroups such as patients with diabetes (*9*) or patients with obesity (*10*). Additionally, it is an optimal resource for evaluating nonperfusion markers. For example, we could evaluate the feasibility and prognostic utility of quantifying right ventricular perfusion (*24*), subendocardial perfusion (*25*), or diastolic parameters. Critically, the registry is designed to facilitate automatic quantitation of novel parameters, allowing it to function as an ongoing source of clinically relevant information.

Although the importance of SPECT MPI perfusion has been extensively studied in REFINE SPECT, the previous registry did not include CTAC imaging data. Engbers et al. demonstrated a stepwise increase in MACEs with increasing CAC among patients with both normal and abnormal perfusion (*26*). Chang et al. identified independent and complementary prognostic information from CAC and myocardial perfusion among 1,126 patients without prior CAD (*27*). Visually estimated CAC also provides risk stratification (*16*). Having the CT images available at the core laboratory facilitates evaluation of the complementary value of anatomic information. For example, we have demonstrated that DL CAC provides independent prognostic value for patients undergoing SPECT/CT MPI (*14*). Similarly, it is possible to improve risk estimation by estimating cardiac chamber volumes from CT (*28*) or by measuring epicardial adipose tissue volume and density (*18*). Adding CTAC images to the registry will lead to important data regarding the incremental utility of these parameters.

The registry will continue to serve as an optimal dataset for developing and validating artificial intelligence applications. The contribution from multiple centers enables study designs that include both internal and external testing, which can now include multiple external sites with the expanded database. Artificial intelligence has been applied to accurately identify patients with abnormal myocardial perfusion using pretest features (*29*) or risk of MACEs (*11*) or to allow automatic rest scan cancellation in patients with a low risk of obstructive CAD (*30*) or MACEs (*31*). The original

registry has also evaluated new artificial intelligence approaches such as unsupervised learning (*32*) and time-to-event predictions (*33*), as well as optimized existing approaches (*34*). Since this registry includes all the imaging datasets, direct analysis of images with deep learning is also possible. These deep learning models can be used to improve identification of obstructive CAD or prediction of cardiovascular risk (*35,36*). Additionally, we have demonstrated that the models can improve physician diagnostic accuracy (*37*). Importantly, the expanding number of clinical sites reflects an increasingly diverse and contemporary patient population, ensuring broad generalizability of the results.

There are some limitations to the REFINE SPECT registry, as by design it aimed for the least common denominator of the available data. Coronary stenosis on invasive coronary angiography is assessed by visual assessment at each site, and visual assessment is known to overestimate the prevalence of functionally significant disease when compared with fractional flow reserve. However, we are using data collected during routine clinical care, in which fractional flow reserve is not often applied. The collected MACE events include all-cause death since the definition of cardiac death can be difficult, particularly among elderly patients with multiple diseases (*38*). There is also potential heterogeneity between centers, as well as interobserver and intercenter variability in visual SPECT interpretation. However, this limitation is mitigated by the availability of image data and objective quantitative analysis of all imaging data, providing an opportunity for more robust external validation of any developed algorithms. In fact, the heterogeneity of the data may be viewed as a significant strength ensuring wide generalizability of any reported results.

CONCLUSION

The updated REFINE SPECT registry will allow advancement of the field of quantitative image analysis and artificial intelligence applications in SPECT MPI and evaluation of various aspects of the diagnostic and prognostic efficacy of the new-generation MPI, including SPECT/CT data.

KEY POINTS

QUESTION: Can the REFINE SPECT registry be updated to include CTAC imaging?

PERTINENT FINDINGS: The registry includes scans from 45,252 patients from 13 centers (55.9% male, 64.7 ± 11.8 y old), including associated CT scans from 13,405 patients. Abnormal stress perfusion and deep learning CAC are associated with an increased risk of MACEs.

IMPLICATIONS FOR PATIENT CARE: The REFINE SPECT registry contains a comprehensive set of imaging and clinical variables that will aid in understanding the value of SPECT MPI, leverage hybrid imaging, and facilitate development of new artificial intelligence tools for improving prediction of adverse outcomes incorporating multimodality imaging.

DISCLOSURE

This research was supported in part by grants R01HL089765 and R35HL161195 from the National Heart, Lung, and Blood Institute at the National Institutes of Health (principal investigator, Piotr Slomka). The content is solely the responsibility of the authors and does not necessarily represent the official views of the National Institutes of Health. Robert Miller received consulting fees and research support from Pfizer. Daniel Berman, Piotr Slomka, and Paul Kavanagh participate in software royalties for quantitative perfusion SPECT software at Cedars–Sinai Medical Center. Piotr Slomka has received research grant support from Siemens Medical Systems and consulting fees from Synektik, SA. Daniel Berman, Sharmila Dorbala, Andrew Einstein, and Edward Miller have served or currently serve as consultants to GE HealthCare. Andrew Einstein has received speaker fees from Ionetix, consulting fees from W. L. Gore & Associates, and authorship fees from Wolters Kluwer Healthcare–UpToDate; has served on a scientific advisory board for Canon Medical Systems; and has received grants to his institution from Attralus, Bruker, Canon Medical Systems, Eidos Therapeutics, Intellia Therapeutics, Ionis Pharmaceuticals, Neovasc, Pfizer, Roche Medical Systems, and W. L. Gore & Associates. Sharmila Dorbala has served as a consultant to Bracco Diagnostics, and her institution has received grant support from Astellas. Marcelo Di Carli has received research grant support from Spectrum Dynamics and consulting honoraria from Sanofi and GE HealthCare. Terrence Ruddy has received research grant support from GE HealthCare and Advanced Accelerator Applications. No other potential conflict of interest relevant to this article was reported.

REFERENCES

1. Lloyd-Jones D, Adams R, Carnethon M, et al. Heart disease and stroke statistics: 2009 update. *Circulation.* 2009;119:480–486.
2. Thompson RC, Al-Mallah MH, Beanlands RSB, et al. ASNC's thoughts on the AHA/ACC chest pain guidelines. *J Nucl Cardiol.* 2022;29:19–23.
3. Alkhybari E, Albeshan S, Alanazi B, et al. Radiation dose assessment for myocardial perfusion imaging. *Tomography.* 2023;9:264–273.
4. Slomka PJ, Betancur J, Liang JX, et al. Rationale and design of the REgistry of Fast Myocardial Perfusion Imaging with NExt generation SPECT. *J Nucl Cardiol.* 2020;27:1010–1021.
5. Otaki Y, Betancur J, Sharir T, et al. 5-year prognostic value of quantitative versus visual MPI in subtle perfusion defects. *JACC Cardiovasc Imaging.* 2020;13:774–785.
6. Miller RJH, Sharir T, Otaki Y, et al. Quantitation of poststress change in ventricular morphology improves risk stratification. *J Nucl Med.* 2021;62:1582–1590.
7. Miller RJH, Hu LH, Gransar H, et al. Transient ischaemic dilation and post-stress wall motion abnormality increase risk in patients with less than moderate ischaemia. *Eur Heart J Cardiovasc Imaging.* 2020;21:567–575.
8. Kuronuma K, Miller RJH, Otaki Y, et al. Prognostic value of phase analysis for predicting adverse cardiac events beyond conventional SPECT variables. *Circ Cardiovasc Imaging.* 2021;14:e012386.
9. Han D, Rozanski A, Gransar H, et al. Myocardial ischemic burden and differences in prognosis among patients with and without diabetes. *Diabetes Care.* 2020;43:453–459.
10. Klein E, Miller RJH, Sharir T, et al. Automated quantitative analysis of CZT SPECT stratifies cardiovascular risk in the obese population. *J Nucl Cardiol.* 2022; 29:727–736.
11. Betancur J, Otaki Y, Motwani M, et al. Prognostic value of combined clinical and myocardial perfusion imaging data using machine learning. *JACC Cardiovasc Imaging.* 2018;11:1000–1009.
12. Betancur J, Commandeur F, Motlagh M, et al. Deep learning for prediction of obstructive disease from fast myocardial perfusion SPECT. *JACC Cardiovasc Imaging.* 2018;11:1654–1663.
13. Dorbala S, Di Carli MF, Delbeke D, et al. SNMMI/ASNC/SCCT guideline for cardiac SPECT/CT and PET/CT 1.0. *J Nucl Med.* 2013;54:1485–1507.
14. Miller RJ, Pieszko K, Shanbhag A, et al. Deep learning coronary artery calcium scores from SPECT/CT attenuation maps improves prediction of major adverse cardiac events. *J Nucl Med.* 2023;64:652–658.
15. Pieszko K, Shanbhag A, Killekar A, et al. Deep learning of coronary calcium scores from PET/CT attenuation maps accurately predicts adverse cardiovascular events. *JACC Cardiovasc Imaging.* 2023;16:675–687.
16. Trpkov C, Savtchenko A, Liang Z, et al. Visually estimated coronary artery calcium score improves SPECT-MPI risk stratification. *Int J Cardiol Heart Vasc.* 2021;35:100827.
17. Feher A, Pieszko K, Miller R, et al. Integration of coronary artery calcium scoring from CT attenuation scans by machine learning improves prediction of adverse

cardiovascular events in patients undergoing SPECT/CT MPI. *J Nucl Cardiol.* 2023;30:590–603.
18. Miller RJH, Shanbhag A, Killekar A, et al. AI-derived epicardial fat measurements improve cardiovascular risk prediction from myocardial perfusion imaging. *NPJ Digit Med.* 2024;7:24.
19. Miller RJH, Bonow RO, Gransar H, et al. Percutaneous or surgical revascularization is associated with survival benefit in stable coronary artery disease. *Eur Heart J Cardiovasc Imaging.* 2020;21:961–970.
20. Thygesen K, Alpert JS, Jaffe AS, et al. Third universal definition of myocardial infarction. *Circulation.* 2012;126:2020–2035.
21. Slomka PJ, Nishina H, Berman DS, et al. Automated quantification of myocardial perfusion SPECT using simplified normal limits. *J Nucl Cardiol.* 2005;12:66–77.
22. Williams MC, Shanbhag AD, Zhou J, et al. Automated vessel specific coronary artery calcification quantification with deep learning in a large multi-center registry. *Eur Heart J Cardiovasc Imaging.* 2024;25:976–985.
23. Azadani PN, Miller RJH, Sharir T, et al. Impact of early revascularization on major adverse cardiovascular events in relation to automatically quantified ischemia. *JACC Cardiovasc Imaging.* 2021;14:644–653.
24. Entezarmahdi SM, Faghihi R, Yazdi M, Shahamiri N, Geramifar P, Haghighatafshar M. QCard-NM: developing a semiautomatic segmentation method for quantitative analysis of the right ventricle in non-gated myocardial perfusion SPECT imaging. *EJNMMI Phys.* 2023;10:21.
25. Vermeltfoort IA, Raijmakers PG, Lubberink M, et al. Feasibility of subendocardial and subepicardial myocardial perfusion measurements in healthy normals with ^{15}O-labeled water and positron emission tomography. *J Nucl Cardiol.* 2011;18:650–656.
26. Engbers EM, Timmer JR, Ottervanger JP, Mouden M, Knollema S, Jager PL. Prognostic value of coronary artery calcium scoring in addition to SPECT MPI in symptomatic patients. *Circ Cardiovasc Imaging.* 2016;9:e003966.
27. Chang SM, Nabi F, Xu J, et al. The coronary artery calcium score and stress myocardial perfusion imaging provide independent and complementary prediction of cardiac risk. *J Am Coll Cardiol.* 2009;54:1872–1882.
28. Miller RJH, Shanbhag A, Killekar A, et al. AI-defined cardiac anatomy improves risk stratification of hybrid perfusion imaging. *JACC Cardiovasc Imaging.* 2024;17:780–791.
29. Miller RJH, Hauser MT, Sharir T, et al. Machine learning to predict abnormal myocardial perfusion from pre-test features. *J Nucl Cardiol.* 2022;29:2393–2403.
30. Eisenberg E, Miller RJH, Hu LH, et al. Diagnostic safety of a machine learning-based automatic patient selection algorithm for stress-only myocardial perfusion SPECT. *J Nucl Cardiol.* 2022;29:2295–2307.
31. Hu LH, Miller RJH, Sharir T, et al. Prognostically safe stress-only single-photon emission computed tomography myocardial perfusion imaging guided by machine learning. *Eur Heart J Cardiovasc Imaging.* 2021;22:705–714.
32. Williams MC, Bednarski BP, Pieszko K, et al. Unsupervised learning to characterize patients with known CAD undergoing MPI. *Eur J Nucl Med Mol Imaging.* 2023;50:2656–2668.
33. Pieszko K, Shanbhag AD, Singh A, et al. Time and event-specific deep learning for personalized risk assessment after cardiac perfusion imaging. *NPJ Digit Med.* 2023;6:78.
34. Rios R, Miller RJH, Hu LH, et al. Determining a minimum set of variables for machine learning cardiovascular event prediction. *Cardiovasc Res.* 2022;118:2152–2164.
35. Otaki Y, Singh A, Kavanagh P, et al. Clinical deployment of explainable artificial intelligence of SPECT for diagnosis of CAD. *JACC Cardiovasc Imaging.* 2022;15:1091–1102.
36. Singh A, Miller RJH, Otaki Y, et al. Direct risk assessment from myocardial perfusion imaging using explainable deep learning. *JACC Cardiovasc Imaging.* 2023;16:209–220.
37. Miller RJH, Kuronuma K, Singh A, et al. Explainable deep learning improves physician interpretation of myocardial perfusion imaging. *J Nucl Med.* 2022;63:1768–1774.
38. Lauer MS, Blackstone EH, Young JB, Topol EJ. Cause of death in clinical research: time for a reassessment? *J Am Coll Cardiol.* 1999;34:618–620.